PCCP

Accepted Manuscript

ROYAL SOCIETY OF CHEMISTRY

www.rsc.org/pccp

Cite this: DOI: 10.1039/c0xx00000x

www.rsc.org/xxxxxx

ARTICLE TYPE

Excited-State Proton Coupled Electron Transfer Between Photolyase and the Damaged DNA Through Water Wire: A Photo-Repair Mechanism

Hongjuan Wang, Xuebo Chen,* Weihai Fang*

Received (in XXX, XXX) Xth XXXXXXXXX 20XX, Accepted Xth XXXXXXXXX 20XX
DOI: 10.1039/b000000x

Photolyase enzyme absorbs blue light to repair the damaged DNA through a cyclic electron transfer reaction. A description of the underlying mechanism has proven to be a challenging issue for both experimental and theoretical studies. In the present work, the combined CASPT2//CASSCF/AMBER (QM/MM) calculations have been performed for the damaged DNA in photolyase. A proton-coupled electron transfer (PCET) mechanism has been determined for restoring cyclobutane pyrimidine dimer (CPD) to two normal thymine bases by irradiation of photolyase. A well-defined water wire between $FADH^-$ and CPD was determined as a bridge to assist the PCET process within $FADH^-$ and thereby trigger the forward electron transfer to CPD. The subsequent CPD splitting and the alternation of the H-bond pattern proceed in a concerted way, which makes the productive backward electron transfer occur on an ultrafast timescale. A local minimum of $S_{CT}(^1\pi\pi^*)$-LMin was identified on the pathway of the futile backward electron transfer (BET), which is stabilized by the strong H-bond interaction between the water wire and CPD. As a result, the futile BET process is endothermic by ~18.0 kcal/mol, which is responsible for 2.4-ns timescale inferred experimentally for the futile BET process. Besides the unbiased interpretation for the majority of the experimental findings, the present study provides new excited-state PCET mechanism that leads to a significant step toward a deeper understanding of the photo-repair process of the damaged-DNA by the photolyase enzyme.

Introduction

Absorption of the solar UV radiation causes DNA mutagenesis and possible tumorigenesis in human skin cells where photo-induced dimerization occurs between two adjacent pyrimidine bases within the same strand.[1] It is generally accepted that the thymine dimerization proceeds through an ultrafast [2+2] photocycloaddition reaction, which starts from an excited electronic state[2-5] and produces cyclobutane pyrimidine dimer (CPD) in the ground state as the final product via the effective nonadiabatic relay in the vicinity of a conical intersection or singlet/triplet crossing.[6-8] Fortunately, most species can survive from the UV light disaster because the damage can be repaired with the aid of the photolyase enzyme. Within the repair process flavin adenine dinucleotide, in its fully reduced form ($FADH^-$), is activated as a catalytic cofactor of the electron donor to split the CPD into the original pyrimidine units upon photo-excitation of the photolyase enzyme with blue light.[9-15]

In the past decades, an electron transfer mechanism has been widely applied to the interpretation of the damaged-DNA repair.[16-24] However, the mechanistic details of the electron tunneling pathways and their influences on the repair efficiency are still unclear. In a benchmark work, Stuchebrukhov and coworkers proposed that the adenine of $FADH^-$ acts as an important intermediate for the indirect ET from the isoalloxazine to thymine bases.[25,26] In this process, the photo-induced ET initially proceeds along the N9-C14 bond (see scheme 1 for atomic numbering) of the $FADH^-$ skeleton, which is followed by the electron tunneling.[25,26] Conversely, Prytkova et al. suggested a direct ET mechanism from the dimethylbenzene side of the isoalloxazine to the dimer through the adjacent methyl group, which rules out the participation of adenine as an intermediate for the electron hop.[27]

Zhong and co-workers reported dynamics and mechanism of the CPD repair by DNA photolyase with femtosecond time-resolved transient spectroscopy.[28,29] The two fundamental processes of electron-tunneling pathways and cyclobutane ring splitting were resolved and adenine was determined to act as an efficient electron-tunneling mediator. The related intermediates and final products were observed and their reaction timescales were determined by monitoring all steps of the repair reaction.[28,29] Real-time measurements reveal that the overall repair is completed in 700 ps through an electron forward-backward transfer cycle, which includes a forward electron transfer (FET) process within 250 ps, the first C5-C5′ bond fission within 10 ps, and the second C6-C6′ bond splitting within 90 ps. In contrast, the time scale of the futile BET without the second-bond breakage was found to be 2.4 ns, one order of magnitude longer than that of the FET process.[28,29] These key experimental findings

reveal a clear spatio-temporal molecular picture of CPD repair by DNA photolyase, although there was a debate concerning the time scale of the futile BET[30] and its influence on the repair quantum yield.[30-36]

As pointed out by Stuchebrukhovin in a commentary on the progress in understanding the damaged-DNA repair by photolyase,[37] the tunneling mechanism proposed by Zhong and coworkers[28,29] is convincing, but not without a question. The first fundamental issue unresolved up to now is why the futile BET process is much slower than its forward counterpart, which is closely related to the repair efficiency by the photolyase enzyme. This difference in kinetics can certainly be attributed to the difference in the mechanisms of the BET and FET processes. The second unresolved issue is associated with an unusual long lifetime of ~1.3 ns observed for $FADH^-$ in the $S_{CT}(^1\pi\pi^*)$ state.[38] The long lifetime implies a slow dissipation of the excited-state energies into protein or water environment, which is one of the key factors for high repair efficiency of the damaged DNA by photolyase. The activation energy was inferred to be 1.9 kJ/mol from the temperature dependence of the splitting reaction of the CPD radical anion in a glycerol/water mixture solution,[39] which is lower than the activation energy of ~43.0 kJ/mol for the overall repair process determined in the enzyme-substrate complex of DNA photolyase.[11] The C6-C6' cleavage was predicted to occur within a few picoseconds for the CPD radical anion in protein or water environment by the hybrid QM/MM[22,40] and *ab inito* MD simulations,[41,42] which is about two orders of magnitude smaller than that observed in the complex of photolyase enzyme with the damaged DNA[28,29] and in flavin−thymine dimer adduct.[43] It remains unclear why the interaction between the enzyme and the substrate can result in such a large change in the rate constant of the C6-C6' bond cleavage, which is the third issue unresolved currently. In addition, the excited-state decay of $FADH^-$ and the CPD splitting were separately explored in previous theoretical studies.[22,27,38,40-42,44-45] No effective correlation has been established between the two dynamic processes, preventing a clear understanding of the photo-repair mechanism of the damaged DNA by photolyase.

Resolution of these issues requires a more detailed probe of the photo-repair mechanism from a theoretical viewpoint. However, this is a topic of a great challenge to electronic structure calculations and dynamics simulations. The combined quantum mechanical/molecular mechanical (QM/MM) approach at the CASPT2//CASSCF/AMBER level has been successfully used to investigate photo-biological processes.[46-48] The same approach is employed in the present work to determine minimum-energy profiles (MEPs) of the excited-state PCET, the CPD splitting, and the other related processes. A well-defined water wire between $FADH^-$ and CPD was determined as a bridge to assist electron tunneling through a bond and the proton-coupled electron transfer within $FADH^-$ was characterized to be the rate-determining step of the overall FET process. After one electron is transferred to 5'-thymine of CPD, the strong H-bond is formed between the water wire and CPD, leading to a deep potential well. As a result, the futile BET process is of high endothermic character, which is responsible for the long timescale observed experimentally for the futile BET process. However, the CPD splitting and the alternation of the H-bond pattern proceed in a concerted way, which makes the productive BET process occur on an ultrafast timescale. We believe that the present study provides new insights into the photo-repair mechanism of the damaged-DNA by the photolyase enzyme, besides the unbiased interpretation for the majority of the experimental findings.

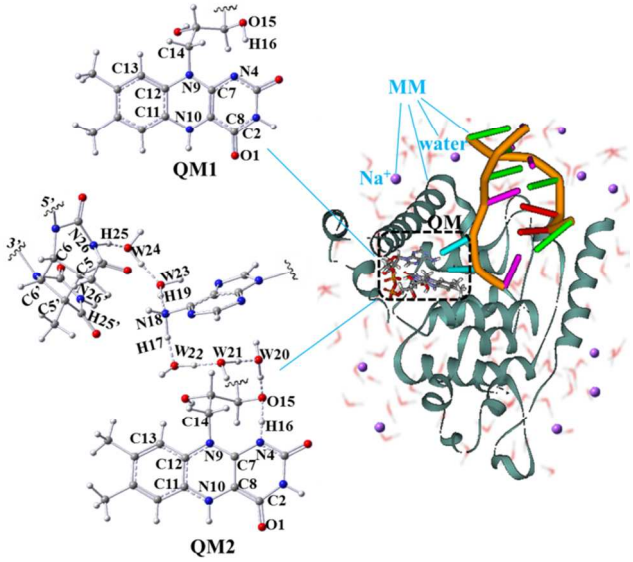

Scheme 1. Illustration of the QM/MM computational model. A part of $FADH^-$ is selected as the QM1 subsystem, while the adenine part of $FADH^-$, the thymine dimer, five water molecules were added into the extended QM2 subsystem. The remaining part of $FADH^-$, amino acid residues, DNA bases, counter-ions Na^+, and water molecules are treated by molecular mechanics

Computational methods

The model system was initially taken from the RCSB Protein Data Bank (PDB) under code name 1TEZ chain A.[49] To reduce the computational cost, residues 1 to 237, which are far from the reaction center, were removed from N-terminal, resulting in a starting structure with 5402 atoms. To keep the whole system electrically neutral, 13 Na^+ counter-ions were added. The AMBER-parm99 force field[50] was employed for the whole system. The undefined parameters of $FADH^-$ were recalculated with the restrained electrostatic potential (RESP) using the tleap module of AMBER10.[51] A cutoff radius of 9Å was used for the real space electrostatic interactions and the van der Waals terms. The system was equilibrated for 1 ns under ambient conditions (NVT ensemble) using the program package TINKER.[52] A cluster analysis of the sampled snapshots generates the appropriate starting structure with intermolecular hydrogen bonds among crystal water molecules and adenine/thymine bases in the reaction center. The two stacked thymine bases of the reaction center in 1TEZ is in their repaired state, which are replaced by the CPD dimer and followed by the QM/MM optimization for the whole system.

As shown in Scheme 1, two different QM/MM partitions were employed in this work. To explicitly describe the first step of the intra-molecular proton transfer, a small QM1 subsystem (40 atoms) representing a portion of $FADH^-$ was used. To comprehensively account for the forward/backward ET and the

Cite this: DOI: 10.1039/c0xx00000x

www.rsc.org/xxxxxx

ARTICLE TYPE

CPD splitting, the adenine part of $FADH^-$, the thymine dimer, and five crystal water molecules were added into the extended QM2 subsystem, resulting in a total of 100 atoms. The MM subsystem includes the remaining part of the $FADH^-$ molecule, DNA bases, amino acid residues, water molecules, and counterions. The calculations of the QM parts were conducted at the complete active space self-consistent field (CASSCF) level of theory. To accurately describe the first step of the intra-molecular proton transfer, the active space of 12 electrons in 10 orbitals (12e/10o) combined with the 6-31G* basis set. Those orbitals include O (15)-H (16) σ/σ* orbitals, N (4) lone-pair n orbital and the rest of 8e/7o originating from high-lying occupied π and low-lying π* orbitals that are mainly distributed in the isoalloxazine moiety. To perform the CASSCF and CASPT2 computations for the QM2 subsystem with 100 atoms, a reduced active space and basis set were adopted to balance the accepted calculation errors and the available computational resources. We excluded some unimportant π and π* orbitals whose occupation numbers are close to 0 or 2, leading to a total of 8 active electrons in 7 active orbitals (8e/7o) in the computations of forward/backward ET and bond-splitting processes. The energy gaps between the excited state and the ground states at reduced level are calculated to be consistent with those obtained at CASPT2/CASSCF(12e/10o) level of theory. To characterize the forward/ backward ET process, a minimum active space of 4e/4o is used to describe the excited state of the isoalloxazine moiety, while the O (N)-H σ/σ* (2e/2o) and corresponding non-bonding lone pair (2e/1o) have to be included. For the bond-splitting process, the related C5-C5' and C6-C6' σ/σ* were used to replace O(N)-H σ/σ* orbitals combined with the high-lying occupied π and low-lying π* orbitals on the $FADH^-$. All of these orbitals in the active space are shown schematically in Figures S1-1 to S1-4.

The local minima and intermediates for the S_0 and $S_{CT}(^1\pi\pi^*)$ states were fully optimized at the CASSCF/AMBER level. The minimum-energy pathways for the proton-coupled forward/backward ET and the CPD splitting were determined by stepwise optimization, in which the reaction coordinate was chosen at different values whereas all the remaining degrees of freedom were fully optimized. Geometry optimizations were performed using a 2-root state-averaged CASSCF approach for the $S_{CT}(^1\pi\pi^*)$ state and a state-specific approach for the S_0 state. Single-point energies at all optimized structures were determined from the 4-root state-averaged CASPT2//CASSCF calculations to include more dynamical electron correlation. These calculations were performed without an ionization potential-electron affinity (IPEA) shift, but including an energy-level shift of 0.2 a.u. to avoid the intruder state problem. The CASSCF and CASPT2 calculations were performed using the Gaussian[53] and Molcas[54] software packages, whereas the AMBER force field was employed using the Tinker[52] tool package. The interface between the QM and MM parts was coded by Ferré et al.[55] and included in the Molcas program. For more computational details see section 1 of the Supporting Information (SI).

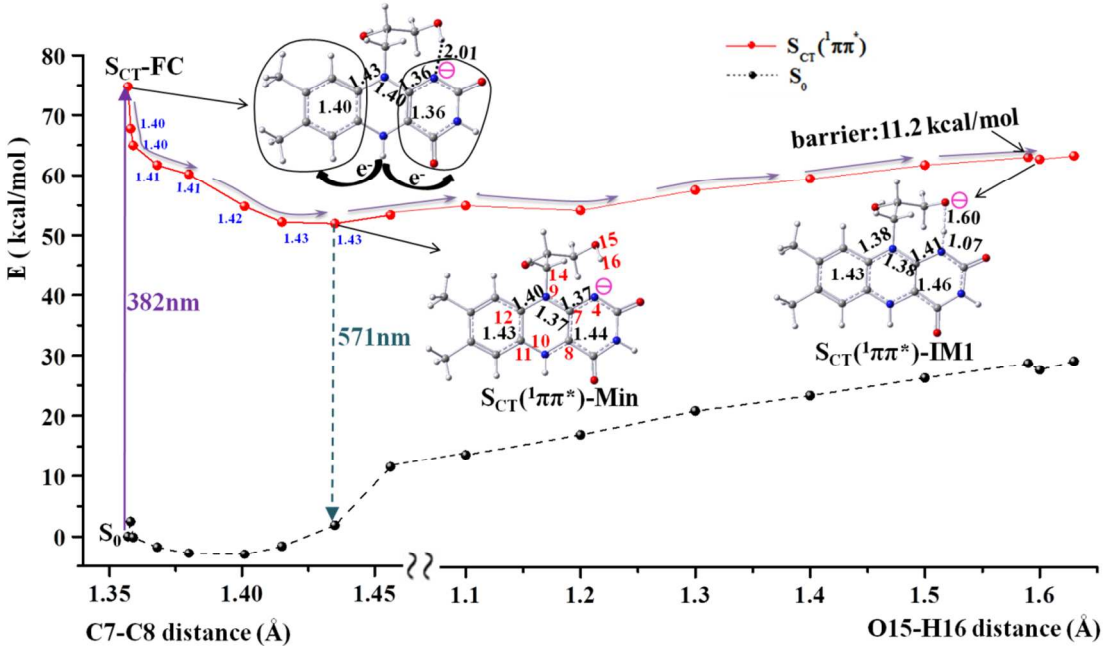

Figure 1. Minimum energy profiles of the initial excited-state relaxation and the subsequent intra-molecular proton transfer in the $S_{CT}(^1\pi\pi^*)$ state upon the 382-nm photoexcitation of $FADH^-$. The C11-C12 distances are shown in blue. The results were obtained by the CASPT2//CASSCF(12e,10o)/Amber QM/MM computation

Cite this: DOI: 10.1039/c0xx00000x

www.rsc.org/xxxxxx

ARTICLE TYPE

Results and discussion

The precursor state of the FET process.

On the basis of the CASSCF(12e,10o)/AMBER optimized S_0 structure, the vertical excitation wavelengths to the lowest three excited singlet states (S_1, S_2, and S_3) were calculated to be respectively 398, 382, and 272 nm at the 4-root state-averaged CASPT2//CASSCF (12e,10o)/AMBER level. A comparison with steady-state absorption shows that the S_2 state is initially populated upon photo-excitation at ~365 nm.[28,38] Based on electronic population analyses (Table S5-1 in SI), the $S_0 \rightarrow S_2$ transition originates from one electron promoted from a π orbital localized on pyrazine to a π^* orbital distributed in the dimethylbenzene and pyrimidine moieties. It is evident that the S_2 state is of the $^1\pi\pi^*$ character. To further explore the property of this state, a charge translocation is calculated on the basis of Mulliken population and an appropriate fragment strategy (section 4 in SI), which reveals that there is -0.4 atomic charge transferred to two moieties of the isoalloxazine ring upon the initial photo-excitation to the S_2 state. In comparison with the S_0 state, negative charge distributed in the N4, C7, and C12 atoms are significantly increased, while there is a considerable decrease of negative charge distributed on the N9 and N10 atoms of the middle pyrazine ring. Therefore, the S_2 state exhibits a partial charge-transfer (CT) character and is referred to as $S_{CT}(^1\pi\pi^*)$. Consistent with the charge redistribution from S_0 to $S_{CT}(^1\pi\pi^*)$, the total dipole moment is calculated to be 72.0 D in the S_0 state and 67.5 D in the $S_{CT}(^1\pi\pi^*)$ state. A small variation of dipole moment from S_0 to $S_{CT}(^1\pi\pi^*)$ was observed in recent experiment.[56] The photo-induced charge transfer in $FADH^-$ produces an unfavorable precursor $S_{CT}(^1\pi\pi^*)$ state for the forward ET through the N9-C14 bond, since less negative charge is distributed in the N9 atom in this state. Conversely, the N4 atom becomes more proton-lacking due to charge redistribution in the $S_{CT}(^1\pi\pi^*)$ state and can function as an acceptor to attract the proton from the adjacent hydroxyl O15-H16 group.

The minimum-energy structure in the $S_{CT}(^1\pi\pi^*)$ state, denoted as $S_{CT}(^1\pi\pi^*)$-Min hereafter, was determined by full optimization at the CASSCF/Amber level and the optimized structure is shown in Figure 1, along with some key bond parameters. In comparison with the $S_{CT}(^1\pi\pi^*)$ Franck-Condon (S_{CT}-FC) structure (the S_0 equilibrium structure), the C7-C8 (1.36→1.44 Å) and C11-C12 (1.40→1.43 Å) bonds are significantly elongated and the N9-C12 and N9-C7 bonds are slightly shortened in the $S_{CT}(^1\pi\pi^*)$-Min structure. This structural deformation gives further evidence that the CT nature of the $S_{CT}(^1\pi\pi^*)$ state is associated with a simultaneous charge transfer along the opposite direction from the middle pyrazine ring to the dimethylbenzene and pyrimidine moieties. As shown in Figure 1, the initial relaxation from the S_{CT}-FC point to $S_{CT}(^1\pi\pi^*)$-Min leads to a sharp decrease in energy from 74.8 to 51.9 kcal/mol. A red-shifted fluorescence at 571 nm can be generated from S_{CT} ($^1\pi\pi^*$)-Min, which is consistent with the experimental observation of weak fluorescence at 545 nm.[38] It should be pointed out that the $S_{CT}(^1\pi\pi^*)$ state becomes the lowest excited singlet state in the $S_{CT}(^1\pi\pi^*)$-Min structure.

As discussed before, negative charge is mainly distributed on the N4 atom in the $S_{CT}(^1\pi\pi^*)$-Min structure. This gives a hint that the H16 proton transfer from O15 to N4 is the dominant channel after relaxation to $S_{CT}(^1\pi\pi^*)$-Min, which is confirmed by the present CASPT2//CASSCF(12e,10o)/Amber calculation.Actually, the intra-molecular N4···H16-O15 hydrogen bond has been found to play a significant role in controlling photochemical properties of $FADH^-$ in DNA photolyase in the previous study.[45] An intermediate on the $S_{CT}(^1\pi\pi^*)$ state, referred to as $S_{CT}(^1\pi\pi^*)$- IM1, was fully optimized at the CASSCF(12e,10o)/Amber level. As shown in Figure 1, the N4-H16 bond is nearly formed in the $S_{CT}(^1\pi\pi^*)$-IM1 structure with the H16···O15 distance of ~1.60 Å. The pathway of the H16 proton transfer from $S_{CT}(^1\pi\pi^*)$-Min to $S_{CT}(^1\pi\pi^*)$-IM1 was characterized by stepwise CASSCF (12e,10o)/Amber optimizations. The $O15^-$ anion is actually generated in $S_{CT}(^1\pi\pi^*)$-IM1, due to departure of the H16 proton, which triggers the subsequent FET process. A barrier of 11.2 kcal/mol is determined on the pathway from $S_{CT}(^1\pi\pi^*)$-Min to $S_{CT}(^1\pi\pi^*)$-IM1, but the reverse process from $S_{CT}(^1\pi\pi^*)$-IM1 to $S_{CT}(^1\pi\pi^*)$-Min is almost barrierless. Thus, $S_{CT}(^1\pi\pi^*)$-IM1 is kinetically unstable and there is little possibility that this intermediate is observed experimentally. The excited-state lifetime of $FADH^-$ in photolyase was experimentally measured to be 1.3 ns.[38] The relatively long excited-state lifetime is consistent with the existence of a noticeable barrier (11.2 kcal/mol) on the pathway from $S_{CT}(^1\pi\pi^*)$-Min to $S_{CT}(^1\pi\pi^*)$-IM1 and a negligible barrier on its reverse process of $S_{CT}(^1\pi\pi^*)$-IM1→$S_{CT}(^1\pi\pi^*)$-Min.

The forward ET process.

Several crystal H_2O molecules exist between $FADH^-$ and CPD in the complex of the photolyase enzyme with the damaged DNA.[49] They can serve as a water wire to achieve long-distance (> 10 Å) electron transfer from the $O15^-$ anion to the CPD acceptor. As shown in Figure 2, the adenine of the $FADH^-$ cofactor lies on the halfway of electron transfer from $O15^-$ to CPD and has been confirmed to function as mediator for electron transfer to substrate in DNA repair.[28,29] A well-defined water wire was determined between $FADH^-$ and CPD, which contains three H_2O molecules (W20, W21 and W22) between the oxygen anion and the adenine and two H_2O molecules (W23 and W24) between the adenine and CPD. The CASSCF/Amber calculations reveal that the forward electron transfer and proton motion proceed in a synchronous concerted way along the lowest excited singlet state that is still labeled by $S_{CT}(^1\pi\pi^*)$. The PCET potential energy profile in the $S_{CT}(^1\pi\pi^*)$ state was determined by the CASPT2//CASSCF/Amber single-point energy calculations on the basis of the CASSCF/Amber optimized structures, which is plotted in Figure 2 as a function of the N18-H17 or N18-H19 distance.

Besides $S_{CT}(^1\pi\pi^*)$-IM1, another two minimum-energy structures were found on the PCET pathway, referred to as $S_{CT}(^1\pi\pi^*)$-IM2 and $S_{CT}(^1\pi\pi^*)$-IM3. The optimized structures for $S_{CT}(^1\pi\pi^*)$-IM1, $S_{CT}(^1\pi\pi^*)$-IM2, and $S_{CT}(^1\pi\pi^*)$-IM3 are given in Figure 2 along with the selected bond parameters. In the $S_{CT}(^1\pi\pi^*)$-IM2 structure, the H17 proton moves away from N18 and the N18···H17 distance (1.44 Å) is longer than that (1.16 Å) in the $S_{CT}(^1\pi\pi^*)$-IM1 structure. Meanwhile, the H19 proton moves toward N18 with the H19···N18 distance shortened to 1.46 Å in the $S_{CT}(^1\pi\pi^*)$-IM2 structure. Further forward proton-coupled electron transfer produces the third intermediate of $S_{CT}(^1\pi\pi^*)$-IM3, in which one electron is transferred to the 5'-thymine of CPD. This is in an agreement with the experimental observation that the forward ET initially reaches the 5′ side of CPD.[28,29]

After passing through a tiny barrier, which was determined to be in close vicinity to the $S_{CT}(^1\pi\pi^*)$-IM1 minimum, the proton-coupled electron transfer occurs first along a downhill pathway to reach the second intermediate of $S_{CT}(^1\pi\pi^*)$-IM2. Then, the third intermediate of $S_{CT}(^1\pi\pi^*)$-IM3 is formed by overcoming a barrier of ~3.0 kcal/mol that is in close proximity to the $S_{CT}(^1\pi\pi^*)$-IM3 minimum. It is evident that the forward electron transfer from $S_{CT}(^1\pi\pi^*)$-IM1 to $S_{CT}(^1\pi\pi^*)$-IM3 is an ultrafast process. Mulliken population analysis reveals that in the $S_{CT}(^1\pi\pi^*)$-IM2 structure there is only -0.5 atomic charge distributed in the NH_2 group of the adenine, while one unit negative charge is transferred to the 5'-thymine of CPD in the $S_{CT}(^1\pi\pi^*)$-IM3 structure. This shows that the forward electron transfer from $S_{CT}(^1\pi\pi^*)$-IM1 to $S_{CT}(^1\pi\pi^*)$-IM3 proceeds in one step and the electron directly tunnels from the cofactor to CPD, although $S_{CT}(^1\pi\pi^*)$-IM2 is a minimum-energy structure on the pathway. As pointed out by Zhong and co-workers in a recent study,[57] the forward ET from the cofactor to the dimer substrate does not follow the hopping mechanism with two tunneling steps from the cofactor to adenine and then to dimer substrate.

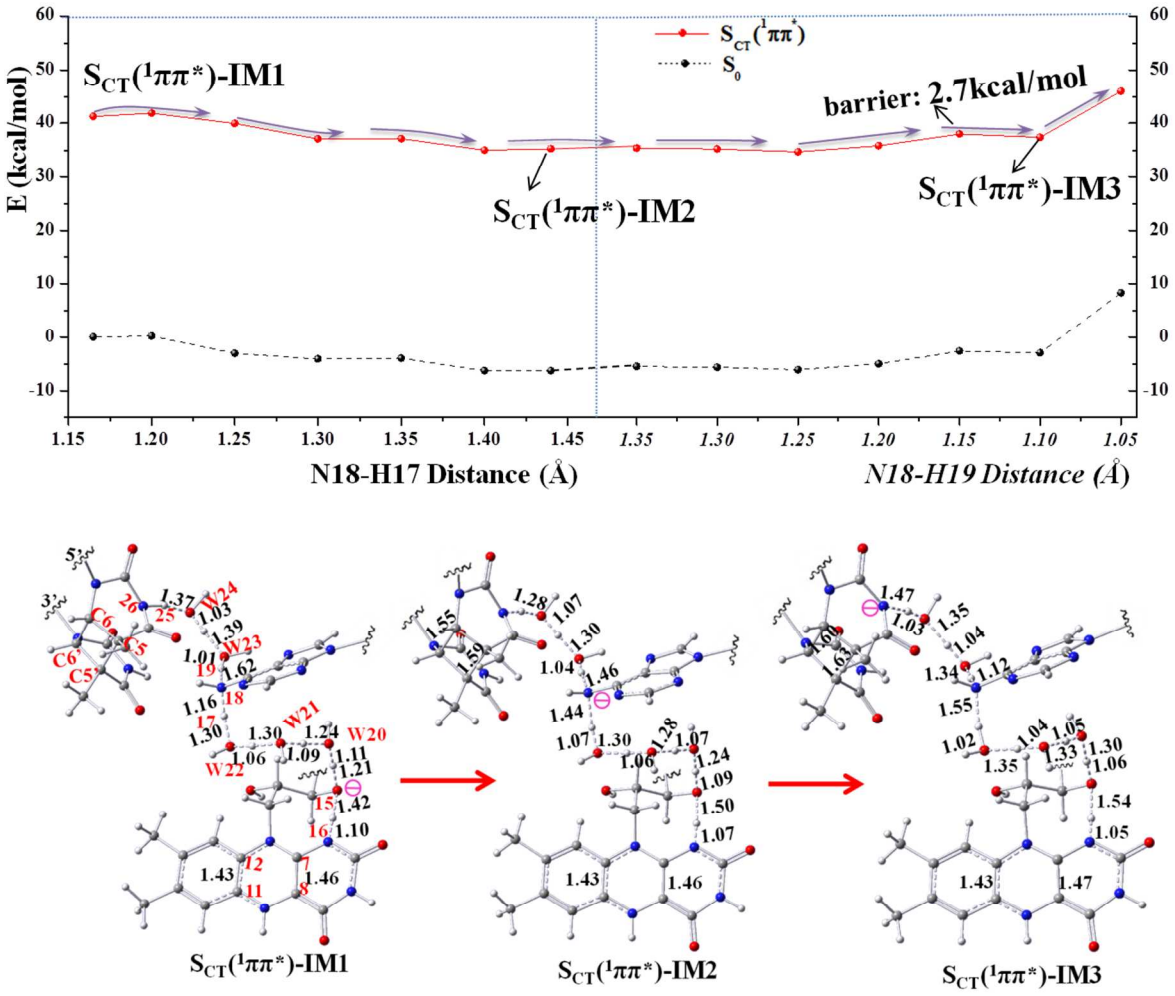

Figure 2. MEPs of the forward electron transfer in the $S_{CT}(^1\pi\pi^*)$ state plotted as a function of the N18-H17 or N18-H19 distance. The $S_{CT}(^1\pi\pi^*)$-IM1, $S_{CT}(^1\pi\pi^*)$-IM2, and $S_{CT}(^1\pi\pi^*)$-IM3 intermediates are schematically shown, together with the numbering scheme and key bond lengths.

In this work, a metallic-like conduction mechanism of ET is proposed to be activated by the mediator of adenine in $FADH^-$ through proton motion to a limited extent along the well-defined water wire. This proposal is supported by the previous studies in which electron tunneling mediated by a water wire has been found to be accelerated by the interposition between the donor and acceptor over a long distance of several water molecules in protein and aqueous media.[58-61] Similar proton-coupled ET mechanism was also suggested to play the decisive role in biological function of FAD containing systems/previous

studies.[46,48,62-64] It should be pointed out that the present PCET mechanism depends on a simultaneous formation of two water wires, N4-water-wire-adenine and adenine-water-wire-CPD. As can be seen from the optimized structures of the three intermediates in Figure 2, the distance of the intermolecular H-bond is within 1.63 Å, which is much shorter than that (2.0 - 2.3 Å) of the normal intermolecular N···H or O···H bond. It is obvious that the H-bond interaction is very strong in the well-defined water wire, due to the concerted effect of many hydrogen bonds. As a result, the barrier height of the FET process is decreased significantly. This explains why a very slow (2.0 ns) forward ET to adenine was observed in the mutation experiment without CPD,[57] in contrast to the forward ET to CPD (250 ps) through adenine relay.[28]

Fission of the first carbon-carbon (C5-C5') bond.

Because of the strong H-bond interaction, the structure of the CPD part in $S_{CT}(^1\pi\pi^*)$-IM3 is different from its radical anion studied before,[22,40-42] although one electron is transferred to the 5'-thymine of CPD. As shown in Figure 3, the C5-C5' bond is initially elongated along with a downhill $S_{CT}(^1\pi\pi^*)$ pathway. Meanwhile, the O24-H25' distance is shortened markedly. There exists only one strong H-bond between W24 and the 5'-thymine with the H25···N26 distance of 1.47 Å in the $S_{CT}(^1\pi\pi^*)$-IM3 structure. Another strong H-bond between W24 and 3'-thymine is formed, when the C5-C5' distance is elongated to 2.10 Å. Formation of the new strong H-bond is responsible for a significant decrease of energy with the initial C5-C5' elongation. However, the further elongation of the C5-C5' distance is prohibited, as indicated in Figure 3 by the rapid rise in energy with an increase of the C5-C5' distance. In this case, either the C6-C6' bond cleavage occurs to release the restriction of the C5-C5' fission, or the C5-C5' bond is reformed with the recovery of the CPD arrangement. Reformation of the C5-C5' bond and the subsequent BET process will be discussed in the following section. It was found that the C6-C6' bond cleavage is triggered by a breakage of the strong H-bond between W24 and the 5'-thymine. To explore this mechanism, the minimum-energy pathway of the O24-H25 bond fission in the $S_{CT}(^1\pi\pi^*)$ state was stepwise optimized and the obtained results are shown in Figure 4 (a). The O24-H25 bond is gradually weakened along the ascending energy profile. The energy maximum appears at a O24···H25 distance of 1.90 Å and the barrier is estimated to be 8.1 kcal/mol. Beyond this maximum, the $S_{CT}(^1\pi\pi^*)$ energy quickly decreases with an increase of the O24-H25 distance, which triggers the second C6-C6' bond cleavage. Consistent with these findings, the trace signal of the C5-C5' bond fission was not detected experimentally and the upper limit of the time constant for this bond fission was estimated to be less than 10.0 ps.[28,29]

The second carbon-carbon (C6-C6') bond cleavage.

The partial fission of the O24-H25 bond and the related alternation of the H-bond pattern result in a cleavage of the C6-C6' bond. As shown in Figure 4 (b) and (c), the C6-C6' bond fission is almost a barrierless process, which is accompanied with

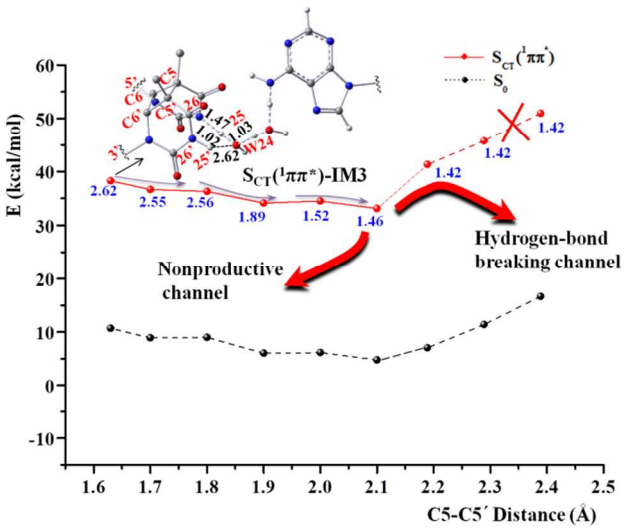

Figure 3. MEP of the first carbon-carbon (C5-C5') bond fission in the S_{CT} ($^1\pi\pi^*$) state along with the O24-H25' distances given in blue.

further elongation of the O24-H25 and C5-C5' bonds. After both the C6-C6' and C5-C5' bonds are elongated to 2.20 Å, the CPD splitting becomes more easier, which occurs along a downhill pathway to the cleaved CPD. More than 30.0 kcal/mol was released after the CPD splitting, which is consistent with a large free energy decrease (> 20.0 kcal/mol) determined in the previous dynamics simulations.[41] Population analysis reveal that the C6-C6' and C5-C5' σ-bonds disappear at their critical distance of 2.20 Å (Section 3 in the SI), which are changed into the two π orbitals that are delocalized over separated thymine bases. As pointed out before, the C6-C6' bond cleavage is triggered by the O24-H25 bond fission and the related change of the H-bond pattern, which is identified as the rate-determining step. A barrier of 8.1 kcal/mol was determined for the rate-determining step. The C6-C6' bond cleavage was experimentally inferred to have a time constant of 90 ps.[28] The present QM/MM calculation reveals that the time constant of 90 ps originates from the barrier on the rate-determining step of the H-bond pattern alternation, which is the pre-step of the C6-C6' bond cleavage.

Productive/futile BET processes.

After the C6-C6' and C5-C5' bonds are broken, the productive BET proceeds smoothly to complete the overall repair. Similarly, the adenine of $FADH^-$ functions as a mediator to switch on the BET process by the distance alternation between proton H17 and the amino group (N18-H17). When the N18-H17 distance is shortened to 1.09 Å, all deviated protons in the FET step return to their original positions. Meanwhile, the CPD is restored to two normal thymine bases. In the complete cycle of CPD repair by photolyase, the forward ET initially reaches the 5′ side of CPD, while the productive BET process starts from the 3′ side. This is consistent with the experimental findings[28,29] that the adenine moiety mediates FET toward the 5′ side of CPD and the electron

Cite this: DOI: 10.1039/c0xx00000x

www.rsc.org/xxxxxx

ARTICLE TYPE

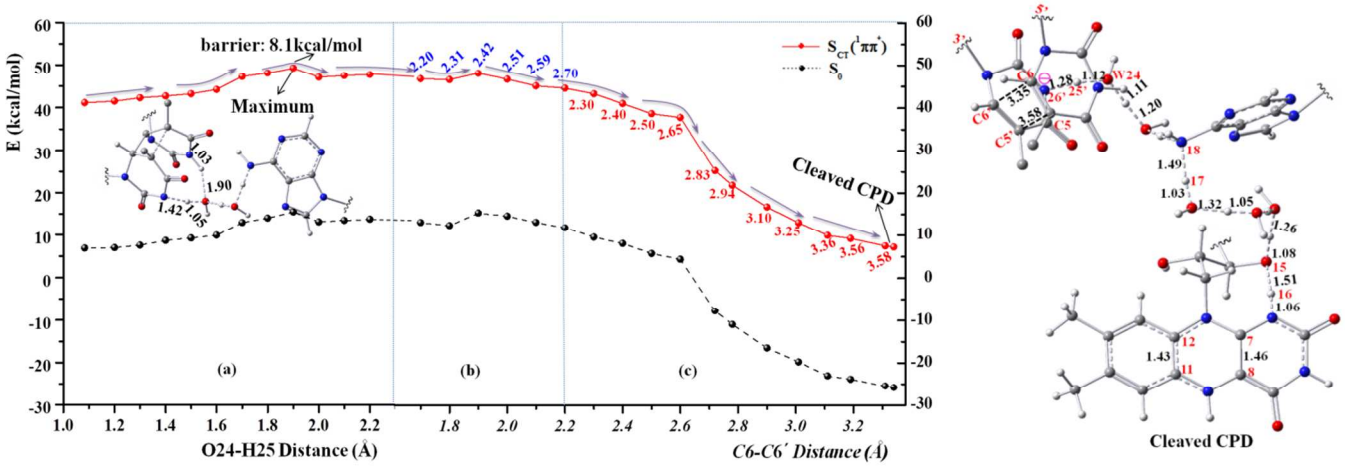

Figure 4. MEPs of the CPD repair in the S_{CT} ($^1\pi\pi^*$) state through (a) hydrogen bond O24-H25 breaking, (b) the concerted hydrogen bond breaking and the C6-C6' bond fission and (c) the asynchronous concerted C6-C6' and C5-C5' bonds splitting. The O24-H25 distance is given in blue and the C5-C5' distance in red. The Maximum and Cleaved CPD is schematically shown with the numbering scheme and key bond lengths, in which some hydrogen atoms are omitted for clarity.

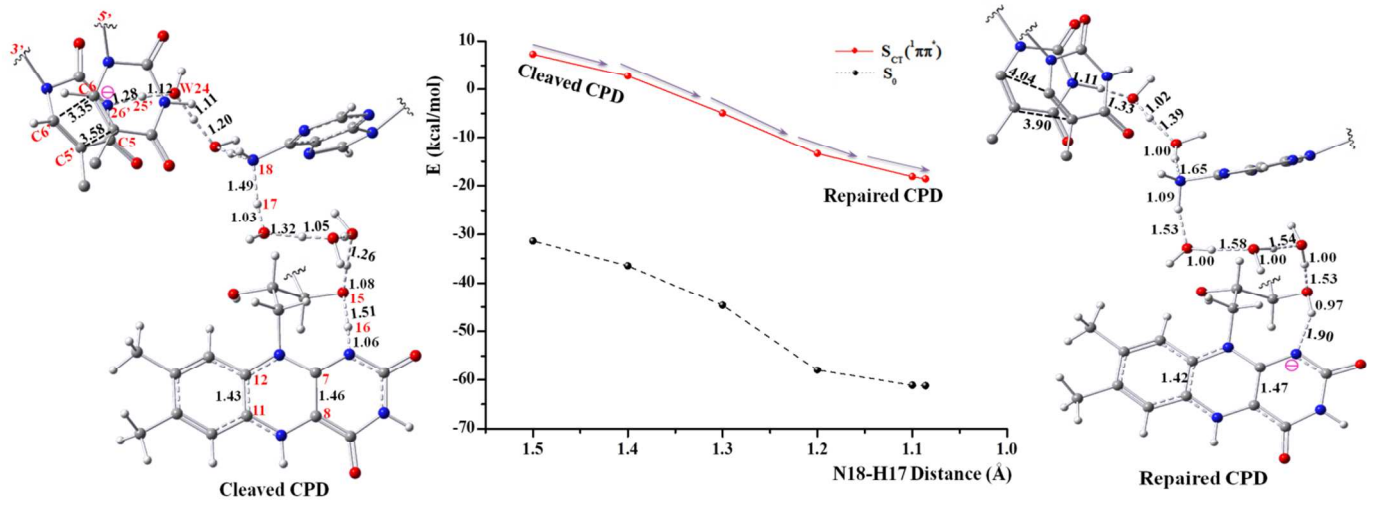

Figure 5. MEP of the productive backward ET in the S_{CT}($^1\pi\pi^*$) state shown along the reaction coordinate of N18-H17 distance. The structures of cleaved and repaired CPD are schematically illustrated with the numbering scheme and key bond lengths.

stays at the 3′ side after the complete breakage of the two C-C bonds. As shown in Figure 5, the productive BET in the S_{CT}($^1\pi\pi^*$)state is predicted to be exothermic by ~25.0 kcal/mol with no barrier on the pathway. Although the backward electron transfer was observed to occur on the ultrafast timescale,[28,29] the time constant of 700.0 ps inferred experimentally is not supported by the present QM/MM calculation.

Before the C6-C6' bond is broken, the BET process can take place and leads to the futile product. A local minimum in the S_{CT}($^1\pi\pi^*$) state was found on the pathway of the futile backward electron transfer, referred to as S_{CT}($^1\pi\pi^*$)-LMin. The S_{CT}($^1\pi\pi^*$)-LMin structure is fully optimized at the CASSCF/Amber level and the obtained result is shown in Figure 6, along with the key bond parameters. The C5-C5' bond is reformed in the S_{CT}($^1\pi\pi^*$)-LMin structure with an intact CPD, which is further stabilized by the existence of two strong H-bonds between W24 and CPD. Actually, the S_{CT}($^1\pi\pi^*$)-LMin minimum is locked by the strong H-bond, which makes the futile BET more difficult. Overall, the futile BET process is endothermic by 17.9 kcal/mol, which can account for the long timescale (2.4 ns) observed experimentally for the futile backward ET process.[28,29]

Cite this: DOI: 10.1039/c0xx00000x

www.rsc.org/xxxxxx

ARTICLE TYPE

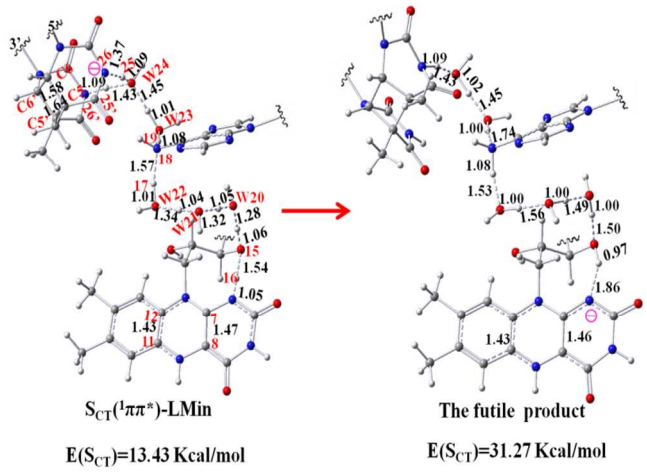

Figure 6. The structures and relative energies of the local minimum with respect to the zero level of ground state minimum and the futile product in the $S_{CT}(^1\pi\pi^*)$ state along with the numbering scheme and key bond lengths.

After one electron is transferred to CPD along the $S_{CT}(^1\pi\pi^*)$ pathway, the two strong hydrogen bonds are formed between CPD and the well-defined water wire, which generates a deep potential well in the $S_{CT}(^1\pi\pi^*)$ state. Since the damaged DNA in photolyase is not repaired and there exists the strong H-bond interaction between CPD and the water wire, a large amount of energies are required in order to achieve the futile backward electron transfer. This is the reason why the futile backward ET process is of high endothermic character. As a result, a long timescale was observed experimentally for the futile BET process. However, the situation is quite different for the productive BET process, where the strong H-bond interaction is significantly weakened and CPD is restored into two normal thymine bases. These processes release more than sufficient energies to compensate for those required for the backward electron transfer. Therefore, the productive BET process exhibits an exothermic character, which occurs much faster than the futile backward ET process.

Finally, it should be pointed out that the photo-cycle of CPD repair by photolyase, which includes the forward ET, the alternation of the H-bond pattern, the CPD splitting, and backward ET, occurs on the $S_{CT}(^1\pi\pi^*)$ state. As can be seen from Figures 1 - 5, the $S_{CT}(^1\pi\pi^*)$ minimum-energy profiles are nearly in parallel with those for the S_0 state and the energy gap of the two states is about 40.0 kcal/mol. Since no conical intersection was found between the $S_{CT}(^1\pi\pi^*)$ and S_0 states, the $S_{CT}(^1\pi\pi^*)\rightarrow S_0$ internal conversion does not occur within an ultrafast timescale, which is consistent with the long lifetime measured experimentally for $FADH^-$ in the $S_{CT}(^1\pi\pi^*)$ state.[38] If the internal conversion was an ultrafast process, the repair efficiency of the photolyase enzyme would be very low. Therefore, the slow dissipation of the $S_{CT}(^1\pi\pi^*)$ energies into protein or water environment plays an important role in the high repair efficiency of the photolyase enzyme.

Conclusions

In the present work, the combined CASPT2//CASSCF /AMBER (QM/MM) calculations have been performed for the damaged DNA in photolyase. A repair mechanism has been determined for restoring cyclobutane pyrimidine dimer (CPD) to two normal thymine bases by irradiation of photolyase with blue light, which involves the forward ET to CPD, the alternation of the H-bond pattern, stepwise C-C breakage of CPD, and the productive backward electron transfer. Upon photo-excitation of $FADH^-$ at ~365 nm, the S_2 state is initially populated, which originates from a promotion of one electron from a π orbital localized on pyrazine to a π^* orbital distributed in the dimethylbenzene and pyrimidine moieties. The S_2 state exhibits a partial CT character, referred to as $S_{CT}(^1\pi\pi^*)$. Consistent with the charge redistribution from S_0 to $S_{CT}(^1\pi\pi^*)$, the total dipole moment is calculated to be 72.0 D in the S_0 state and 67.5 D in the $S_{CT}(^1\pi\pi^*)$ state. A small variation of dipole moment from S_0 to $S_{CT}(^1\pi\pi^*)$ was observed in recent experiment.[56] The $S_{CT}(^1\pi\pi^*)$-Min structure was determined by full optimization at the CASSCF/Amber level and in this structure the $S_{CT}(^1\pi\pi^*)$ state becomes the lowest excited singlet state. The photo-induced charge redistribution in $FADH^-$ produces a favorable precursor state of $S_{CT}(^1\pi\pi^*)$ for the forward electron transfer through the N4···H16-O15 hydrogen bond.

As the first step of the forward electron transfer, the intramolecular proton-coupled electron transfer occurs, generating the $S_{CT}(^1\pi\pi^*)$-IM1 intermediate with one electron transferred to the O15 atom ($O15^-$ anion). A barrier of 11.2 kcal/mol is determined on the pathway from $S_{CT}(^1\pi\pi^*)$-Min to $S_{CT}(^1\pi\pi^*)$-IM1, but the reverse process from $S_{CT}(^1\pi\pi^*)$-IM1 to $S_{CT}(^1\pi\pi^*)$-Min is almost barrierless. Thus, $S_{CT}(^1\pi\pi^*)$-IM1 is kinetically unstable and there is little possibility that this intermediate is observed experimentally. A well-defined water wire was determined between $FADH^-$ and CPD, which functions as a bridge for the forward ET from the $O15^-$ anion to the adenine and then to CPD. The forward ET process from $S_{CT}(^1\pi\pi^*)$-IM1 proceeds in one step on the $S_{CT}(^1\pi\pi^*)$ state with a barrier of ~3.0 kcal/mol. This process leads to formation of $S_{CT}(^1\pi\pi^*)$-IM3 as a product, where one electron is transferred to 5'-side of CPD. It is evident that the generation of the $O15^-$ anion is the rate-determining step for the whole FET process. The existence of a barrier of 11.2 kcal/mol on the rate-determining step is consistent with a time constant of 250 ps inferred experimentally for the FET process.[28]

After one electron is transferred to 5'-thymine of CPD, one strong H-bond is formed between W24 and the 5'-thymine. Subsequently, the first C5-C5' bond cleavage is accompanied with formation of another strong H-bond between W24 and the 3'-thymine. As a result, the C5-C5' cleavage proceeds along the

Cite this: DOI: 10.1039/c0xx00000x

www.rsc.org/xxxxxx

ARTICLE TYPE

downhill pathway. Actually, the upper limit of the time constant was estimated to be less than 10.0 ps for the C5-C5' bond fission.[28,29] There is no barrier for the second C6-C6' bond cleavage, however, a barrier of 8.1 kcal/mol was determined for breaking the strong H-bond between W24 and the 5'-thymine, which triggers fission of the C6-C6' bond. The time constant of 90.0 ps inferred experimentally[28,29] for fission of the C6-C6' bond originates probably from the barrier on the pathway of breaking the H-bond between W24 and the 5'-thymine.

A local minimum of $S_{CT}(^1\pi\pi^*)$-LMin was found on the pathway of the futile backward electron transfer. Besides reformation of the C5-C5' bond, $S_{CT}(^1\pi\pi^*)$-LMin is further stabilized by the existence of two strong H-bonds between W24 and CPD. As a result, the futile BET process is endothermic by 17.9 kcal/mol, which can account for the long timescale (2.4 ns) observed experimentally for the futile BET process.[28,29] However, the situation is quite different for the productive BET process, where the strong H-bond interaction is significantly weakened and CPD is restored into two normal thymine bases. These processes release energies more than enough to compensate for those required for the backward electron transfer. This is the reason why the productive BET process exhibits an exothermic character and occurs much faster than the futile BET process. Finally, it should be pointed out that no conical intersection was found between the $S_{CT}(^1\pi\pi^*)$ and S_0 states and the $S_{CT}(^1\pi\pi^*)\rightarrow S_0$ internal conversion does not occur efficiently. Thus, the photo-cycle of CPD repair by photolyase occurs on the $S_{CT}(^1\pi\pi^*)$ state, which is consistent with the long lifetime measured experimentally for $FADH^-$ in the $S_{CT}(^1\pi\pi^*)$ state. More importantly, the slow dissipation of the $S_{CT}(^1\pi\pi^*)$ energies into protein or water environment is one of the key factors for high repair efficiency of the photolyase enzyme.

Acknowledgements

This work was supported by grants from the NSFC (Grant No. 20973025 and 21373029) and from the Major State Basic Research Development Programs (Grant No. 2011CB808503).

Notes and references

Key Laboratory of Theoretical and Computational Photochemistry of Ministry of Education, Department of Chemistry, Beijing Normal University, Xin-wai-da-jie No. 19, Beijing, 100875, China, Emails: xuebochen@bnu.edu.cn fangwh@bnu.edu.cn

References

1 J. Cadet, P. Vigny, In Bioorganic Photochemistry: Photochemistry and the Nucleic Acids; H. Ed. Morrison, Wiley: New York, 1900; pp 1-272.

2 W. J . Schreier, T. E. Schrader, F. O. Koller, P. Gilch, C. E. Crespo Hernández, V. N. Swaminathan, T. Carell, W. Zinth, B. Kohler, *Science,* 2007, **315**, 625-629.

3 W. J. Schreier, J. Kubon, N. Regner, K. Haiser, T. E. Schrader, W. Zinth, P. Clivio, P. Gilch, *J. Am. Chem. Soc.,* 2009, **131**, 5038-5039.

4 A. Banyasz, T. Douki, R. Improta, T. Gustavsson, D. Onidas, I. Vayá, M. Perron, D. Markovitsi, *J. Am. Chem. Soc.,* 2012, **134**, 14834-14845.

5 W. M. Kwok, C. Ma, D. L. Phillips, *J. Am. Chem. Soc.,* 2008, **130**, 5131-5139.

6 M. Boggio-Pasqua, G. Groenhof, L. V. Schäfer, H. Grubmüller, M. A. Robb, *J. Am. Chem. Soc.*, 2007, **129**, 10996-10997.

7 T. Climent, I. González-Ramírez, R. González-Luque, M. Merchán, L. Serrano-Andrés, *J. Phys. Chem.* Lett., 2010, **1**, 2072-2076.

8 D. Roca-Sanjuan, G. Olaso-González, M. Rubio, P. B. Coto, M. Merchán, V. Ludwig, L. Serrano-Andrés, L. *Pure Appl. Chem.,* 2009, **81**, 743-754.

9 R. Dulbecco, *Nature*, 1949, **163**, 949-950.

10 M. Byrdin, V. Sartor, A. P. Eker, M. H. Vos, C. Aubert, K. Brettel, P. Mathis, *Biochim. Biophys. Acta.,* 2004, **1655**,*64-70.*

11 T. Langenbacher, X. Zhao, G. Bieser, P. F. Heelis, A. Sancar, M. E. Michel-Beyerle, *J. Am. Chem. Soc.,* 1997, **119**, 10532-10536.

12 T. Domratcheva, *J. Am. Chem. Soc.*, 2011, **133**, 18172-18182.

13 Y. T. Kao, C. Saxena, L. J. Wang, A. Sancar, D. P. Zhong, *Cell Biochem. Biophys.,* 2007, **48**,*32-44* .

14 A. Sancar, *Chem. Soc. Rev.,* 2003, **103,** 2203-2237.

15 Y.-T. Kao, C. Saxena, L. Wang, A. Sancar, D. Zhong, *Proc. Natl. Acad. Sci. U.S.A.,* 2005, **102***, 16128-16132.*

16 C. Pac, J. Kubo, T. Majima, H. Sakurai, *Photochem. Photobiol.*, 1982, **36**, 273-282.

17 S. E. Rokita, C. T. Walsh, *J. Am. Chem. Soc.,* 1984, **106**, 4589-4595.

18 R. F. Hartman, J. R. Van Camp, S. D. Rose, *J. Org. Chem.*, 1987, **52**, 2684-2689.

19 P. F. Heelis, D. J. Deeble, S.-T. Kim, A. Sancar, *Int. J. Radiat. Biol.,* 1992, **62**, 137-143.

20 S.-T. Kim, M. Volk, G. Rousseau, P. F. Heelis, A. Sancar, M. E. Michel-Beyerle, *J. Am. Chem. Soc.,* 1994, **116**, 3115-3116.

21 S.-T. Kim, A. Sancar, C. Essenbacher, G. T. Babcock, *J. Am. Chem. Soc.* 1992, **114**, 4442-4443.

22 F. Masson, T. Laino, U. Rothlisberger, J. Hutter , *ChemPhysChem,* 2009, **10**, 400–410.

23 L. O. Essen, T. Klar, *Cell. Mol. Life Sci.,* 2006, **63**, 1266−1277.

24 N. J. Saettel, O. Wiest, *J. Am. Chem. Soc.,* 2001, **123**, 2693-2694.

25 J. Antony, D. M. Medvedev, A. A. Stuchebrukhov, *J. Am. Chem. Soc*., 2000, **122**, 1057-1065.

26 D. Medvedev, A. A. Stuchebrukhov, *J. Theor. Biol.,* 2001**, 210**, 237–248.

27 T. R. Prytkova, D. N. Beratan, S. S. Skourtis, *Proc. Natl. Acad. Sci. U.S.A.,* 2007, **104**, 802-807.

28 Z. Liu, C. Tan, X. Guo, Y.-T. Kao, J. Li, L. Wang, A. Sancar, D. Zhong, *Proc. Natl. Acad. Sci. U.S.A.,* 2011, **108***, 14831-14836.*

29 Z. Liu, X. Guo, C. Tan, J. Li, Y.-T. Kao, L. Wang, A. Sancar, D. Zhong, *J. Am. Chem. Soc.,* 2012, **134**, 8104-8114.

30 K. Brettel, M. Byrdin, *Proc. Natl. Acad. Sci. U.S.A.,* 2012, **109**, E1462.

31 K. Brettel, M. Byrdin, *Curr. Opin. Struct. Biol.,* 2010, **20**, 693–701.

32 W. Harm, *Mutat. Res*., 1970, **10**, 277-290.

33 G. Payne, A. Sancar, *Biochemistry*, 1990, **29**, 7715-7727.

34 A. J. Ramsey, J. L. Alderfer, M. S. Jorns, *Biochemistry,* 1992, **31**, 7134-7142.

35 S.-T. Kim, A. Sancar, *Biochemistry,* 1991, **30**, 8623-8630.

36 D. Zhong, A. Sancar, A. Stuchebrukhov, *Proc. Natl. Acad. Sci. U.S.A.,* 2012, **109**, E1463.

37 A. Stuchebrukhov, *Proc. Natl. Acad. Sci. U.S.A.,* 2011, **108**, 19445-19446.

Cite this: DOI: 10.1039/c0xx00000x

www.rsc.org/xxxxxx

ARTICLE TYPE

38 Y.-T. Kao, C. Saxena, T.-F. He, L. Guo, L. Wang, A. Sancar, D. Zhong, *J. Am. Chem. Soc.,* 2008, **130**, 13132-13139.

39 Q.-H. Song, W.-J. Tang, X.-B. Ji, H.-B. Wang, Q.-X. Guo, *Chem.-Eur. J*., 2007, **13**, 7762−7770.

40 F. Masson, T. Laino, I. Tavernelli, U. Rothlisberger, J. Hutter, *J. Am. Chem. Soc.,* 2008, **130**, 3443-3450.

41 A. A. Hassanali, D. Zhong, S. J. Singer, *J. Phys. Chem. B*, 2011, **115**, 3848−3859.

42 A. A. Hassanali, D. Zhong, S. J. Singer, *J. Phys. Chem. B,* 2011, ***115***, 3860−3871.

43 Y.-T. Kao, Q.-H. Song, C. Saxena, L. Wang, D. Zhong, *J. Am. Chem. Soc.,* 2012, **134**, 1501-1503.

44 A. Acocella, G. A. Jones, F. Zerbetto, *J. Phys. Chem. B,* 2010, **114**, 4101–4106.

45 Y.-J. Ai, F. Zhang, S.-F. Chen, Y. Luo, W.-H. Fang, *J. Phys. Chem. Lett.,* 2010, **1**, 743−747.

46 I. A. Solov'yov, T. Domratcheva, A. R. Moughal Shahi, K. Schulten, *J. Am. Chem. Soc*., 2012, **134**, 18046−18052.

47 A. R. Moughal Shahi, T. Domratcheva, *J. Chem. Theory Comput*., 2013, **9**, 4644–4652.

48 M. G. Khrenova, A. V. Nemukhin, T. Domratcheva, *J. Phys. Chem. B,* 2013, **117**, 2369-2377.

49 A. Mees, T. Klar, P. Gnau, U. Hennecke, A. P. M. Eker, T. Carell, L. O. Essen, *Science,* 2004, **306**, 1789-1793.

50 J. M. Wang, P. Cieplak, P. A. Kollman, *J. Comput. Chem.*, 2000, **21**, 1049-1074.

51 D. A. Case, T. A. Darden, T. E. Cheatham III, C. L. Simmerling, J. Wang, R. E. Duke, R. Luo, K. M. Merz, D. A. Pearlman, M. Crowley, R. C. Walker, W. Zhang, B. Wang, S. Hayik, A. Roitberg, G. Seabra, K. F. Wong, F. Paesani, X. Wu, S. Brozell, V. Tsui, H. Gohlke, L. Yang, C. Tan, J. Mongan, V. Hornak, G. Cui, P. Beroza, D. H. Mathews, C. Schafmeister, W.S. Ross, P.A. Kollman, AMBER 10, University of California, San Francisco, 2008.

52 J. W. Ponder, F. M. Richards. *J. Comput. Chem.*, 1987, **8**, 1016-1024.

53 Gaussian 03, Revision D.02, M. J. Frisch, G. W. Trucks, H. B. Schlegel, G. E. Scuseria, M. A. Robb, J. R. Cheeseman, J. A. Montgomery, Jr., T. Vreven, K. N. Kudin, J. C. Burant, J. M. Millam, S. S. Iyengar, J. Tomasi, V. Barone, B. Mennucci, M. Cossi, G. Scalmani, N. Rega, G. A. Petersson, H. Nakatsuji, M. Hada, M. Ehara, K. Toyota, R. Fukuda, J. Hasegawa, M. Ishida, T. Nakajima, Y. Honda, O. Kitao, H. Nakai, M. Klene, X. Li, J. E. Knox, H. P. Hratchian, J. B. Cross, V. Bakken, C. Adamo, J. Jaramillo, R. Gomperts, R. E. Stratmann, O. Yazyev, A. J. Austin, R. Cammi, C. Pomelli, J. W. Ochterski, P. Y. Ayala, K. Morokuma, G. A. Voth, P. Salvador, J. J. Dannenberg, V. G. Zakrzewski, S. Dapprich, A. D. Daniels, M. C. Strain, O. Farkas, D. K. Malick, A. D. Rabuck, K. Raghavachari, J. B. Foresman, J. V. Ortiz, Q. Cui, A. G. Baboul, S. Clifford, J. Cioslowski, B. B. Stefanov, G. Liu, A. Liashenko, P. Piskorz, I. Komaromi, R. L. Martin, D. J. Fox, T. Keith, M. A. Al-Laham, C. Y. Peng, A. Nanayakkara, M. Challacombe, P. M. W. Gill, B. Johnson, W. Chen, M. W. Wong, C. Gonzalez and J. A. Pople, Gaussian, Inc., Wallingford CT, 2004

54 F. Aquilante, L. De Vico, N. Ferré, G. Ghigo, P.-Å. Malmqvist, P. Neogrády, T. B. Pedersen, M. Pitoňák, M. Reiher, B. O. Roos, L. Serrano-Andrés, M. Urban, V. Veryazov, R. Lindh, *J. Comput. Chem*., 2010, **31**, 224.

55 N. Ferré, A. Cembran, M. Garavelli, M. Olivucci. *Theo. Chem. Acc.*, 2004, **112**, 335-341.

56 C.-W. Chang, L. Guo, Y.-T. Kao, J. Li, C. Tan, T. Li, C. Saxena, Z. Liu, L. Wang, A. Sancar, D. Zhong, *Proc. Natl. Acad. Sci. U.S.A.,* 2010, **107**, 2914−2919.

57 Z. Liu, M. Zhang, X. Guo, C. Tan, J. Li, L. Wang, A. Sancar, D. Zhong, *Proc. Natl. Acad. Sci. U.S.A*., 2013, **110**, 12972−12977.

58 J. Lin, I. A. Balabin, D. N. Beratan, *Science*, 2005, **310**, 1311-1313.

59 T. Hayashi, A. A. Stuchebrukhov, *Proc. Natl. Acad. Sci. U.S.A.,* 2010, **107**, 19157−19162.

60 A. A. Stuchebrukhov, *Phys. Rev. E*, 2009, **79**, 031927.

61 D. N. Beratan, S. S. Skourtis, I. A. Balabin, A. Balaeff, S. Keinan, R. Venkatramani, D. Q. Xiao, *Acc. Chem. Res*., 2009, **42**, 1669–1678.

62 I. A. Solov'yov, T. Domratcheva, K. Schulten, *Sci. Rep.,* 2014, **4**, 3845.

63 J. M. Mayer, D. A. Hrovat, J. L. Thomas, W. T. Borden, *J. Am. Chem. Soc*., 2002, **124**, 11142−11147.

64 M. Lingwood, J. R. Hammond, D. A. Hrovat, J. M. Mayer, T. W. Borden, *J. Chem. Theory Comput*., 2006, **2**, 740−7.

Graphical abstract

A Photo-Repair Mechanism was proposed to proceed through proton-coupled electron transfer controlled by intervening adenine and the assistant of water wire.